ADVANCES IN GEODESY AND GEOINFORMATION
(formerly GEODESY AND CARTOGRAPHY)
Vol. 73, no. 1, article no. e51, 2024


https://doi.org/10.24425/agg.2023.146163

*Original paper*

# Assessment of noise magnitude and velocity uncertainty in continuous GNSS coordinate time series

**Ahmed Mohammed**

Modibbo Adama University, Yola, Nigeria
e-mail: ahmed.mohammed@mau.edu.ng; ORCID: http://orcid.org/0000-0002-7038-3153

Received: 2024-02-22 / Accepted: 2024-04-30

**Abstract:** Global Navigation Satellite Systems (GNSS) technology has emerged as a powerful tool for unraveling Earth's dynamic nature, offering continuous and precise monitoring of geodetic positions with global coverage. This study quantifies the noise magnitude and velocity uncertainty estimates using GNSS-derived coordinate time series data from 31 IGS global stations. It assessed the relationship between the noise level and the uncertainties related to the derived velocities and systematically evaluated the influence of different coordinate solution time spans, satellite orbit/clock products, and GNSS constellation on the noise level and velocity uncertainties. The result gives insights into GNSS velocity estimation, noise characteristics, and the influence of ambiguity resolution. The results suggested that resolving ambiguities and using specific GNSS constellation satellite orbits and clocks solutions enhances the precision of velocity estimates and reduces noise magnitude. The noise levels are observed to be consistently above –0.7 in 5-year solution sets and below –0.8 in 8-year solution sets. There is an average of 30 and 42% reduction in velocity uncertainties due to 3 year increment in solution span using JPL and ESA orbits, respectively. GPS-only solution set appeared to be favorable for high-precision GNSS-based geodynamic applications with increased favourability when the ambiguities are resolved. The identified noise model, GGM+WN, demonstrated the most appropriate noise model in most cases which is not out of place to have been used in quantifying the noise magnitude and velocity uncertainties in this study.

**Keywords:** time-series analysis, continuous GNSS station, Precise Point Positioning, velocity uncertainties, noise properties

## 1. Introduction

Understanding Earth's dynamic nature is crucial for a multitude of endeavors, ranging from hazard mitigation and resource management to fundamental insights into planetary processes. Global Navigation Satellite Systems (GNSS) technology has emerged as a powerful

tool for unraveling these dynamics, offering continuous and precise monitoring of geodetic positions with global coverage (Grapenthin, 2020). GNSS receivers collect measurements of satellite signals, allowing users to estimate positions with millimeter-level accuracy over short timescales. However, the GNSS positioning process is inherently stochastic, affected by various error sources like tropospheric delays, instrumental noise, and multipath reflections (He et al., 2017). These errors manifest as noise in the derived coordinate time series, leading to uncertainties in their analysis. While short-term variations can be smoothed out, estimating long-term trends like Earth's subtle movements requires careful consideration of noise and its impact on velocity uncertainties (Tregoning and Rizos, 2006).

One of the objectives of time series modeling in geodynamic studies is to evaluate a linear or long-term trend. This trend assessment is influenced by the uncertainty, which is primarily determined by the noise at the lowest observed periods or high frequencies (Bos et al., 2008; Bevis and Brown, 2014; He et al., 2018, 2019). However, accurately estimating the noise becomes challenging when only a few data points are used for the longest periods. The empirical covariance matrix estimation may not provide an accurate representation of the noise, as it relies on the first and last observations to compute the noise variance over the longest period. To address this challenge, one approach is to define a noise model and fit the time series data to this model. By estimating the parameters of the noise model relative to the time series, the noise can be better characterized and quantified. The log-likelihood method, along with a numerical maximization strategy, can be employed to estimate the parameters of the noise model (Khanzadi et al., 2011; McCusker et al., 2011). Alternatively, other approaches such as least-squares variance component estimation and Power Spectral Density (PSD) analysis are also available for this purpose (Bos et al., 2020).

The daily variation in coordinate time series has recently proven to be mostly non-random which makes the traditional assumption that the noise in the time series is purely white noise unrealistic. Johnson and Agnew (1995) indicate that GNSS time series noise demonstrates temporal correlation and that the noise's PSD can be well described by a power-law noise model using Eq. 1:

$$P(f) = P_0 \left( \frac{f}{f_s} \right)^k \tag{1}$$

where $f$ is the frequency and $P$ is the PSD. The amplitude and reference frequency are represented by the constants $P_0$ and $f_s$, respectively, while the spectral index is denoted by $k$. The noise's type is indicated by the $k$ value, which when analyzed using integer value could be 0 for white noise (pure random behavior), –1 for flicker noise or –2 for random-walk noise. Occasionally, the term colored noise is used to refer to any form of noise that is not white in nature such as flicker and random-walk noise according to Klos et al. (2018). Some studies (e.g. Santamaría-Gómez et al., 2011; Bogusz and Klos, 2016; Klos et al., 2018) has shown that non-accounting for the specific colored noise present in GNSS coordinate time series data tends to affect the station position and velocity determination because the uncertainties of the parameter estimates can be underestimated by a significant magnitude.

Previous studies on the noise characteristics in GNSS coordinate time series has revealed the presence of power-law noise, often combined with white noise and flicker noise (e.g. Amiri-Simkooei et al., 2007; He et al., 2019; Santamaría-Gómez and Ray, 2021). The noise color in the GNSS coordinate time series is not fixed and can become whiter over time, although the origin of this colored noise and its whitening remains unclear (Santamaría-Gómez and Ray, 2021). Mao et al. (1999) and Goudarzi et al. (2015) both found that a combination of white and flicker noise best characterizes the noise in Global Positioning System (GPS) coordinate time series, with the latter also noting a higher white noise in the vertical component for tropical stations. Amiri-Simkooei et al. (2007) proposed a methodology for assessing noise in GPS coordinate time series, identifying the presence of annual and semi-annual signals and the need to include autoregressive noise in the stochastic model. Amiri-Simkooei (2016) further refined this methodology, introducing non-negative least-squares variance component estimation to simultaneously estimate the amplitudes of different noise components, and confirming the presence of white and flicker noise in GPS time series, with a significant proportion also containing random walk noise. Kaczmarek and Kontny (2018) used wavelet analysis to identify the noise model in GNSS station coordinates, finding that the nature of noise in measurement data does not depend on the signal estimation method. Bos et al. (2013) describe the methodology of evaluating noise characteristics in GNSS coordinate time series data in the presence of systematic variables such as velocity, annual and semi-annual seasonality, and offsets due to equipment change.

Recent research has made significant advancements in GNSS observation and velocity modeling. Zhu (2020) proposed two real-time instantaneous velocity determination methods based on moving-window polynomial modeling, which were found to outperform existing methods. Benoist et al. (2020) demonstrated the benefits of using a spatiotemporal covariance model to estimate station velocities, showing improved accuracy compared to traditional methods. Ding et al. (2020) constructed a time-varying 3-D displacement model, which was found to significantly reduce a ~5.9-year signal in GPS time series. The uncertainty of GNSS site velocity estimates is influenced by the type of noise in the data. This noise can significantly impact the estimation of velocities from GNSS time series, particularly at low frequencies (He et al. 2019). The presence of offsets in the time series can further complicate the noise characteristics, leading to potential underestimation of velocity uncertainties (e.g. Santamaría-Gómez and Ray, 2021). Wang and Herring, (2019) found that position offsets have a limited impact on these uncertainties, while Klos et al. (2014) highlighted the prevalence of flicker noise in GPS time series, which can lead to underestimation of velocity uncertainties. Langbein (2020) proposed a new method for estimating velocity precision, which was found to be less computationally demanding and more accurate for flicker noise. Calais (1999) also identified spatially and temporally correlated noise in GPS data, leading to velocity uncertainties of around 2–3 mm/yr. These studies collectively underscore the importance of considering noise characteristics in GNSS data when estimating velocity uncertainties.

The focus of this study lies in quantifying the noise magnitude in GNSS-derived coordinate time series data, estimating the GNSS station velocity with their formal uncertainties, and systematically evaluating the relationship between the noise magnitude

and the uncertainties associated with the derived velocities. Understanding this relationship is crucial for interpreting GNSS-derived velocities with confidence. Inflated uncertainties due to underestimated noise can lead to spurious interpretations of Earth's dynamics, potentially impacting vital decisions based on geodetic data. By exploring the intricacies of noise and its consequences for velocity estimation, this study aims to contribute to a more robust and reliable interpretation of GNSS-derived insights into Earth's dynamic behavior.

## 2. GNSS data processing strategy

This study sourced 24-hour RINEX (Receiver INdependent EXchange) observation files for 31 International GNSS Service (IGS) global stations (see Fig. 1) from the Crustal Dynamics Data Information System (CDDIS; Noll, 2010). The 31 IGS stations selected adhere to specific criteria: Firstly, they are integral to the IGS core sites crucial for realizing both the ITRF2008 and ITRF2014 frames (Altamimi et al., 2011; 2016), as well as for generating satellite precise orbits and clock corrections utilized by numerous IGS Analysis Centers (ACs). Secondly, the limited number of stations ensures that data processing can be feasibly accomplished within a reasonable timeframe, particularly when contrasted with IGS ACs employing hundreds of stations owing to their superior computational capabilities. Thirdly, these stations are essential for assessing noise and velocity uncertainty stemming from varied GNSS constellation solutions, particularly GPS and GLONASS/GLO, as they track dual-frequency signals from both systems. Fourthly, their strategic distribution across the globe ensures comprehensive coverage of diverse geographic regions, thereby mitigating potential biases originating from localized phenomena. Finally, all the stations lie beyond tectonic active zones, ensuring their stability and displaying consistent linear motion. The observations are for 8 years for a period window from epoch 2010.0 to 2018.0 within which the stations are tracking GPS and GLO dual frequency signals.

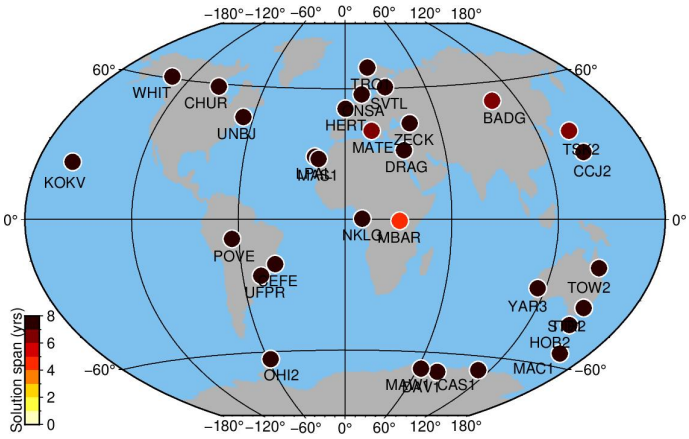


Fig. 1. Spatial distribution of sites used in this study showing clean solution time span for each site for epochs from 2010.0 to 2018.0

GipsyX/RTGx (GipsyX; Bertiger et al., 2020) version 2.1 software package from the Jet Propulsion Laboratory (JPL) was used in processing the RINEX observation files. The processing was undertaken at the geodesy lab of the Surveying and Geoinformatics Department, Modibbo Adama University, Yola which is a GipsyX-licensed institution. Using P1/P2 pseudo-range and linearly combined ionospheric-free (Melbourne, 1985; Wübbena, 1985) L1/L2 carrier phase data, the Precise Point Positioning (PPP) method was used to estimate station coordinates every 24 hours (Zumberge et al., 1997; Kouba and Héroux, 2001) at a processing interval of 300 seconds. The choice of PPP rather than the classical double-differenced (DD) baseline/network processing technique is that it is faster, requires lower computer memory, and achieves the same processing precision as the DD method when used with high-precision satellite orbits, satellite clock corrections, and more advanced geophysical models (Bertiger et al., 2010). Since JPL does not provide multi-constellation precise orbit and clock solutions containing GLO, Center for Orbit Determination in Europe (CODE/COD; Sušnik et al., 2016) and European Space Agency (ESA; Springer et al., 2014) orbits and clock correction were individually sourced and converted to internal GipsyX format before used in the analysis. The station coordinates were then solved using PPP by fixing to the COD and ESA precise orbit and clock corrections respectively. Other sets of GPS-only station coordinates were generated by fixing to some sets of JPL orbit and clock corrections (Desai et al., 2014; Ries et al., 2017; Ries, 2019) for validation purposes.

The orbit/clock solutions and absolute antenna calibrations in the IGS08 or IGS14 reference frames were appropriately switched between different processing runs, where necessary, to get separate solution sets. All solution sets generated are ambiguity-float solutions except for one whose ambiguities were resolved using Wide-Lane and Phase Bias (WLPB) parameters provided by the JPL based on Bertiger et al. (2010). Common geophysical models used in the GNSS data processing include solid Earth and polar tide corrections following the International Earth Rotation and Reference Systems Service 2010 (IERS2010) conventions standards (Petit and Luzum, 2010). Ocean tidal loading was applied using the FES2004 ocean tidal model with the Centre of Mass Correction (CMC) based on Lyard et al. (2006) containing the eleven principal semi-diurnal, diurnal, and long period tidal constituents. Global Mapping Function (GMF) for the troposphere was applied using a random walk process according to Boehm et al. (2006). All solutions were processed with a minimum elevation cut-off angle of 7 degrees which is the standard for generating the orbit and clock solutions used in this study by the relevant IGS ACs. 8-year solution sets (2010.0 – 2018.0) were generated using ESA and JPL products, while only 5-year solutions (2010.0 – 2015.0) were generated using COD products due to discontinuation of the COD products in GPS Week 1827 (3rd week of January 2015). Table 1 provide the summary of all the solution sets generated in this study.

In each solution set generation, station geocentric coordinates and Zenith Total Delays (ZTD) and its gradients in East and North directions at each station were estimated. The estimated geocentric coordinates with their formal errors were organized into time series, converted to local topocentric (dE, dN, and dU) equivalents, and detrended to detect outliers. Outliers were detected using the Median Absolute Deviation (MAD) which is a robust

Table 1. Summary of solution sets generated. The abbreviations G, R, flo, and fix represent GPS, GLO, ambiguity-float, and ambiguity-fixed, respectively

| Solution | Orbit/Clocks | System | Antex file | Ambiguities | Span |
|---|---|---|---|---|---|
| COD G | CODE (Sušnik et al., 2016) | GPS-only | igs08.atx | Float | 5-years |
| COD G+R | | GPS+GLO | igs08.atx | Float | 5-years |
| COD R | | GLO-only | igs08.atx | Float | 5-years |
| ESA G | ESA (Springer et al., 2014) | GPS-only | igs08.atx | Float | 5 and 8-years |
| ESA G+R | | GPS+GLO | igs08.atx | Float | 5 and 8-years |
| ESA R | | GLO-only | igs08.atx | Float | 5 and 8-years |
| JPLi08 flo | JPL (Desai et al., 2014; Ries et al., 2017; Ries, 2019) | GPS-only | igs08.atx | Float | 5 and 8-years |
| JPLi14 flo | | GPS-only | igs14.atx | Float | 5 and 8-years |
| JPLi14 fix | | GPS-only | igs14.atx | Fixed | 5 and 8-years |

measure of the variability of a data set (Singh and Kundu, 2022). By using the median instead of the mean, MAD becomes less affected by outliers or non-normally distributed data. It is particularly useful when dealing with skewed distributions or when the presence of extreme values might distort the results. The MAD (see Eq. 2) calculates the median value of the absolute deviations from the median, providing a measure of dispersion that is more resilient to extreme observations compared to methods like standard deviation, which rely on the mean. The MAD of the detrended residuals in each coordinate component was computed to identify outliers in each station time series (Singh and Kundu, 2022):

$$\mathrm{MAD} = \mathrm{median}\left[|x_i - x_m|\right] \tag{2}$$

whereby, $x_i$ is the coordinate of the observation station at epoch $i$, and $x_m$ is the middle value in the batch of the coordinates in the solution time series.

In this study, outliers are defined as epochs whose residual value in any coordinate component exceeds five times the MAD. The outliers were removed using the same algorithm for all the solution sets. The percentage of the difference between the number of processed daily solutions and cleaned daily solutions is returned as a percentage outlier per site for each solution set. The mean, median, 95%ile, and other statistics were estimated for the outliers and presented in Table 2 and Figure 2. The cleaned solution set span (in years) for each analyzed station for single constellation ESA and JPL solution sets are presented in Fig. 3. An example of detrended stochastic coordinate data for the CEFE (lat = −20.3°; long = 319.7°) station is provided in Figure 4.

All the analyzed stations were observed to have an outlier of less than 1.5% in all solution sets except for the MATE station, which has around 2.5% in all its 5-year solution sets. The overall median value of the outlier for all solution sets ranges from the minimum of 0.2% in JPL orbit solutions to a maximum of 1.5% in ESA orbit solutions (see Table 2 and Fig. 2). The result also shows JPLi08 solution has the lowest interquartile range in the stacked stations outliers while the COD R solution was found to have the highest

Table 2. Percentage outlier statistics for 5-year solution sets

| Statistic | Percentage outlier (%) | | | | | | | | |
|---|---|---|---|---|---|---|---|---|---|
| | COD G | COD G+R | COD R | ESA G | ESA G+R | ESA R | JPLi08 flo | JPLi14 flo | JPLi14 fix |
| Min | 0.06 | 0.06 | 0.13 | 0.32 | 0.38 | 0.13 | 0.00 | 0.00 | 0.00 |
| Max | 4.10 | 6.54 | 6.48 | 3.59 | 2.93 | 2.89 | 4.15 | 4.91 | 7.21 |
| Median | 0.57 | 1.34 | 1.14 | 1.20 | 1.49 | 1.47 | 0.24 | 0.19 | 0.20 |
| Mean | 0.76 | 1.56 | 1.71 | 1.30 | 1.55 | 1.41 | 0.59 | 0.66 | 0.76 |
| 95%ile | 1.83 | 4.75 | 5.31 | 2.46 | 2.62 | 2.33 | 3.10 | 3.37 | 3.49 |

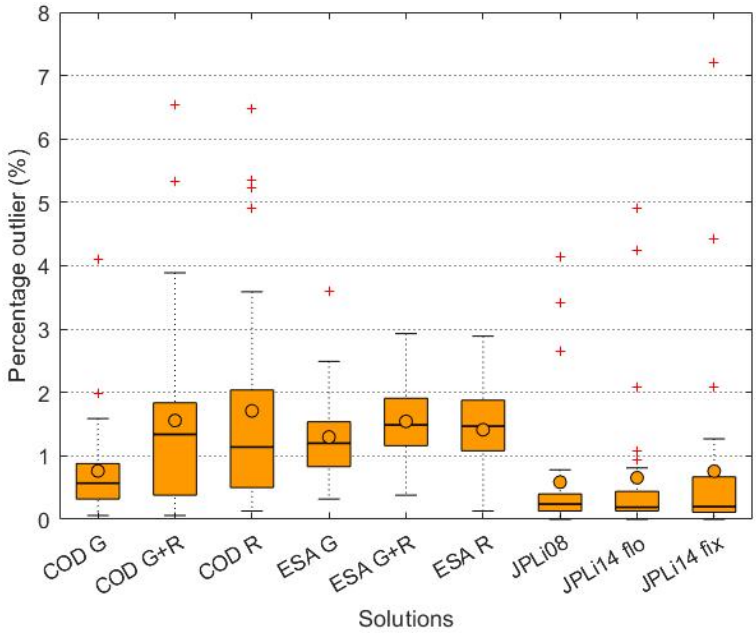


Fig. 2. Mean comparison of percentage outlier between 5-year solutions

interquartile range in the stacked stations outliers. This is an indication that station outliers for the GLO-only solution from the COD orbit are more dispersed than the GPS-only solution from the JPLi08 orbit which show a consistent number of outliers across the stations.

Significant solution gaps were observed on some stations such as DRAG, KOKV, MBAR, NKLG, POVE, and STR2 stations (see Fig. 3). The gaps are primarily due to RINEX observation files' unavailability for those stations on those days at the CDDIS data archive. The remaining gaps are entirely outliers detected using the outlier criteria specified above which were then removed from each station time series data.

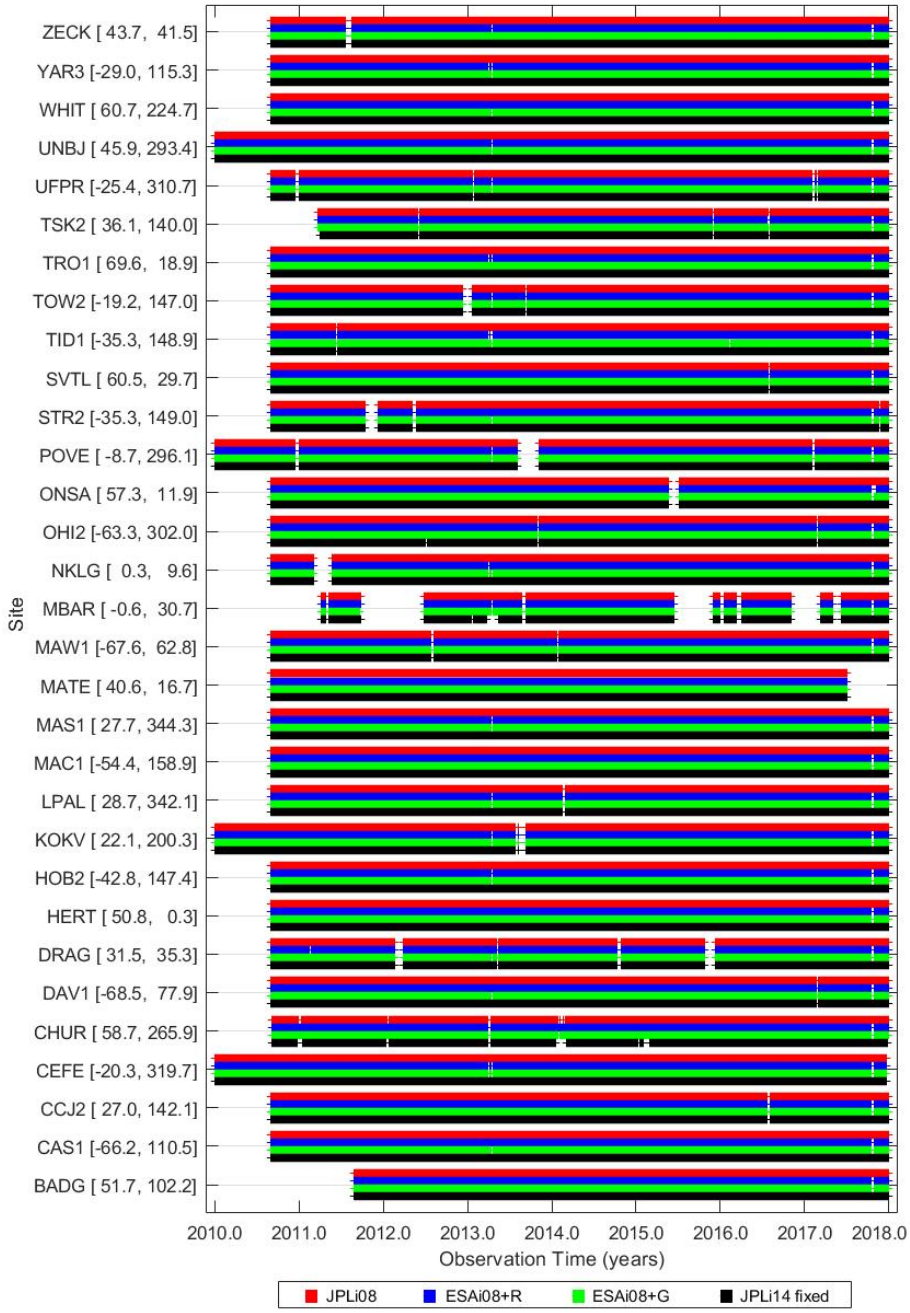


Fig. 3. Locations (latitude and longitude) of sites and their time span for some clean 24 hour batch single constellation PPP solutions

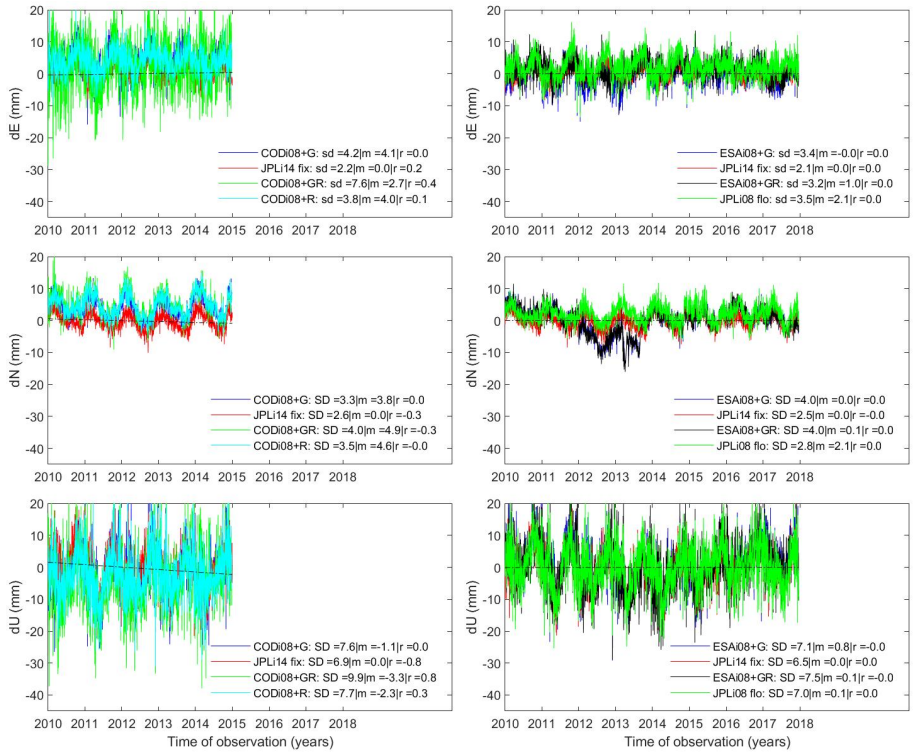


Fig. 4. Detrended residual time series stochastic data of CEFE (Jacutuquara, Brazil) for some of the 5-years solution sets in left panels and 8-years solution sets in the right panels. The standard deviation (SD) and mean offsets relative to reference solution (JPLi14 fix – JPL product on ITRF2014 frame) are in millimeters while the estimated velocity (r) is in mm/yr in which case they are all zeroes because they are for detrended time series data

Most of the station coordinate time series show the presence of trend due to tectonic motion, and annual and semiannual signals with an amplitude ranging from 5 mm to 10 mm in the horizontal coordinate component and from 5 mm to 25 mm in the Up coordinate component. Some stations show the presence of offset due to equipment change. The result in Figure 4 shows the detrended stochastic coordinate data for the CEFE station with an average annual signal of 8 mm across all solution sets in the horizontal coordinate component and an average of 14 mm annual signal in the Up coordinate component. Noise can also be observed from the time series data, especially those containing GLO solution, but their noise characteristics cannot be determined at this stage without undertaking appropriate noise analysis.

## 3. Concept of noise and velocity modeling

For noise and velocity analysis using the "*Estimatetrend*" sub-program in Hector software (Bos et al., 2008; 2013), the coordinate time series of each site can be used to estimate both the model parameters and the chosen noise model parameters using the Maximum

Likelihood Estimation (MLE) method. These model parameters can include trends, annual and semiannual signals (periods of 365.25 and 182.63 days), offsets, and post-seismic deformation (see Eq. 3), according to Bos et al. (2013).

$$x(t) = x_{\mathrm{R}} + v(t - t_{\mathrm{R}}) + \sum_{j=1}^{n_J} b_j \mathrm{H}(t - t_j) + \sum_{k=1}^{n_F} [s_k \sin(\omega_k t) + c_k \cos(\omega_k t)] + \varepsilon_x(t) \quad (3)$$

whereby, the term $x(t)$ refers to the station position at observation epoch $t$, $x_{\mathrm{R}}$ is the reference position at time $t$ =0, $t_R$ is the reference time, and $v$ is the velocity parameter. To allow for one or more offsets due to equipment change at a specific epoch $\{t_j\}$, $j = 1 : n_J$, the second term in the right-hand side (RHS) of Eq. 3 is introduced called the offset term where $b_j$ represents the offset at epoch $t_j$, while the $H$ represents the Heaviside function, sometimes known as the "unit step". To allow for the modeling of seasonality, the third term in the RHS is introduced where the number of frequencies utilised to describe the annual and semi-annual seasonal cycles is denoted by the symbol $n_F$. with $\omega_k = 2\pi/\tau_k$, and $\tau_1 = 1$ year. The noise part is denoted by $\varepsilon_x$ while the remaining unknown parameters $b_k$, $s_k$, $c_k$, $x_R$, and $v$ are solved by fitting the stochastic coordinate time series data to the systems of a functional model given in Eq. 3. The discrete observations epochs needed to form the systems of the functional model above should not be less than 2.5 years long to reduce the effect of seasonal cycles on the velocity bias, as indicated by Blewitt and Lavallée, (2002).

Among the functionalities of Hector software, one can specify the velocity, seasonal, and other periodic signals in the control-file. One can also set in the control-file if another optional parameter is to be estimated, such as offsets, breaks, and/or post-seismic deformation. These are kinds of global model parameters that are usually applied to all time series. On the other hand, the time of an offset, break, or post-seismic deformation differs from station to station is a kind of local model parameter. In Hector, this information is usually written in the header of the time series input file. "*Estimatetrend*" output is categorized into two, viz:

1. Parameters that defined the estimated time series model: include velocity, uncertainty, bias, noise magnitude (spectral index – $k$), amplitude, and phase, among others.
2. Parameters that defined the chosen noise model: include likelihood values, model fraction, spectral index, etc.

With nine separate solution sets generated in this study, it is more prudent to analyze and evaluate them using the estimated parameters in (1) above to determine which one best suits the main task at hand, quantifying the noise magnitude and estimating the velocity with their formal uncertainties.

### *3.1. Empirical evaluation of noise and velocity uncertainties using the GGM+WN model*

It is a well-known fact that velocity uncertainty and noise level (spectral index – $k$) significantly impact geodynamic studies. One can compare the solution sets based on either noise level magnitude or velocity uncertainty level between various solution sets

generated. Still, for a more robust comparison, one can employ linear regression analysis between the two estimated parameters (noise level and velocity uncertainty). To achieve linearity between the two variables in the regression, the records were sorted by the dependent variable (noise level). Any station that exabit a non-linear motion ($k$ value in the random walk noise region) will appear as an outlier in the linear regression graph and should be removed from the analysis since it is outside the scope of this study to analyze the non-linear velocities. However, to work with estimated k values that will cover the entire noise region ($0 \geq k \geq -3$: $k$ representing noise from white to random walk value), this study works with a non-stationary power-law noise model. The non-stationary power-law noise analysis can be achieved in Hector using the Generalized Gauss–Markov plus White Noise (GGM+WN) combination with GGM_1mphi coefficient fixed to a value of 6.9e–06 (Bos et al., 2008; 2013). The time series of each station position component (north, east, up) are treated independently. The assessment technique of the different solution sets generated in this study can best be described by the simulated Figure 5.

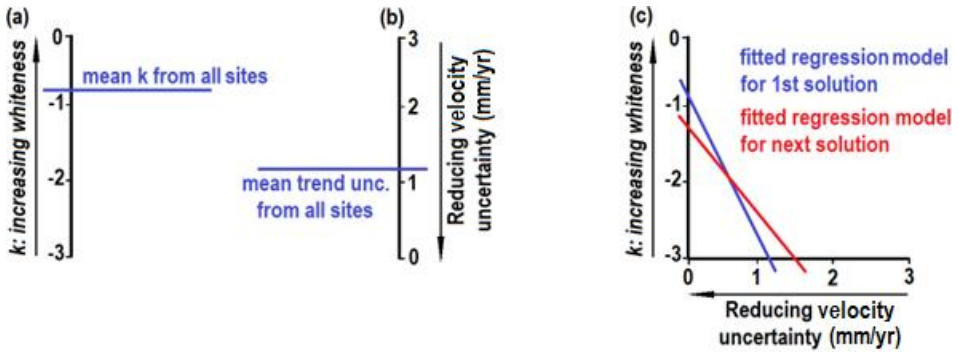


Fig. 5. Simulated representation of the research objective, which tries to detect the whitest noise solution and the least velocity uncertainty through a robust linear regression concept

In Figure 5a and Figure 5b, the assessment is 1-dimensional while the 2-dimensional assessment concept is illustrated in Figure 5c, which graphically shows the best analysis solution set for geodynamic studies. The fitted regression model with the steepest slope among the solution sets is the best in whiteness and the lowest velocity uncertainty. A practical interpretation of Figure 5c will provide rich information that will help decide on the solutions. For instance, their intersection point will define the noise and velocity uncertainty level at which both solutions agree. The empirical comparisons of the stacked mean estimated spectral indices from all stations (see Fig. 1) are presented in Figure 6a and Figure 6b for 5-year and 8-year solution sets respectively.

The results show that, except for the ESA solution in the horizontal component, the noise level results from Fig. 6a randomly averaged above –0.7 in all the 5-year solution sets and below –0.8 in 8-year solution sets. This indicates that the noise magnitude increase with an increase in the solution span used in modeling the noise and other parameters for both single and combined constellation solution sets. For 5-year GPS-only solution sets, COD and JPL orbits produced solutions with lower noise levels with median values of

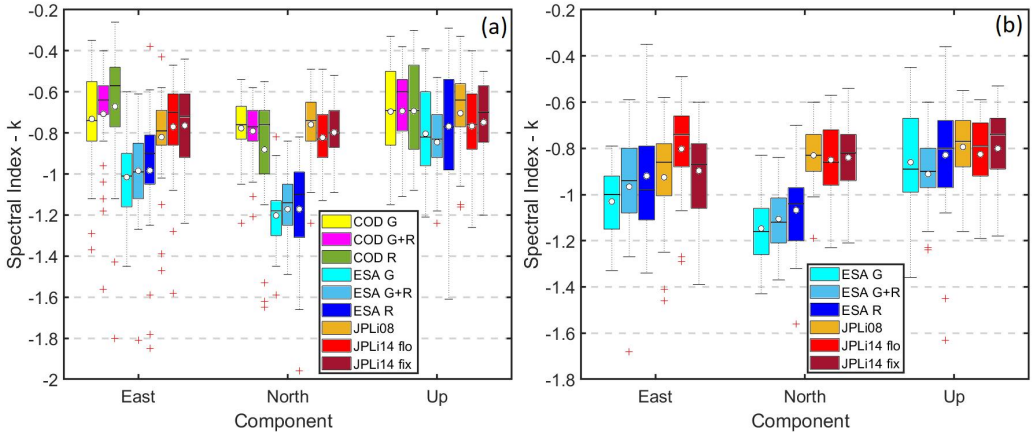


Fig. 6. Stacked mean spectral indices for 5-year solutions in (a) and 8-year solutions in (b) estimated using GGM+WN noise model combination

–0.69 and –0.64, respectively, compared to –0.82 in ESA equivalent in the Up component. The same applies to 8-year solution sets where JPL orbits produced GPS-only solution sets lower median noise level value of –0.77 compared to –0.89 in ESA orbits solutions. It could also be noticed from Fig. 6 how JPL on i08 frames produced a lower noise level in the Up component compared to JPL on i14 frame. However, applying ambiguity resolution improved the noise level in i14 frame solutions for both 5 and 8-year solution sets. In both 5 and 8-year solution sets, GLO only solution noise magnitude was observed to be slightly less than either the GPS only or the combined GPS+GLO solution noise magnitude. This may likely be explained by the lower number of satellite observations used in the modeling of the GLO only solution than in the GPS only or the combined GPS+GLO solution. One thing to note here is that the estimates compared in Fig. 6 may be biased because the GGM+WN noise model may not be 100% best fit for all the solution sets.

The empirical comparisons of the stacked mean estimated velocity uncertainties from all stations (see Fig. 1) are presented in Figure 7a and Figure 7b for 5-year and 8-year solution sets respectively.

As with the noise level, the velocity uncertainties produced using ESA orbits and clock solutions are larger than those produced using COD or JPL in all coordinate components (see Fig. 7a). The velocity uncertainties in the Up components are 2 to 3 times in magnitude compared to those in the average horizontal components. There is an average of 30 and 42% reduction in velocity uncertainties due to 3 years increment in solution span using JPL and ESA orbits, respectively. Combined GPS+GLO solutions from both COD and ESA were observed to slightly reduce the mean values of the velocity uncertainties in all coordinates components compared to their corresponding single constellation (either GPS-only or GLO-only) solution sets, except for COD 5-year solution in the East component, as can be seen in Figure 7. As with the spectral index, the velocity uncertainty estimates in Figure 7 may be biased because the GGM+WN noise model may not be 100% best fit for the entire solution sets.

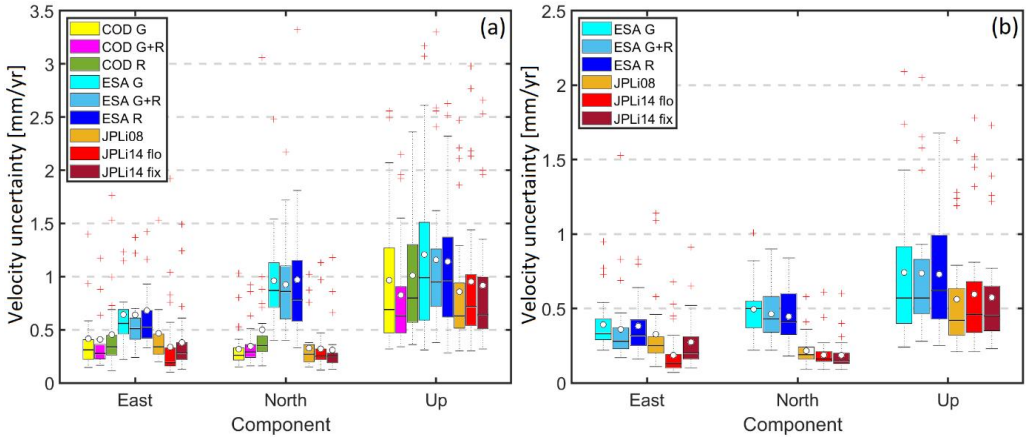


Fig. 7. Stacked mean velocity uncertainty for 5-year solutions in (a) and 8-year solutions in (b) estimated using GGM+WN noise model combination

This study analyzed the regression model fit between the spectral index and velocity uncertainty contributions from all stations for each solution set to see a more robust comparison between the solution sets. The regression analysis excludes inputs from stations with spectral indices in the Random Walk noise region. The results are summarized in Figure 8.

The result from Figure 8 shows that the steepness of the model line for all solution sets in the horizontal component is more than the Up components indicating higher positioning precision and lower noise magnitude in the East and North components compared to the Up component. Except in the East components of 5-year solution sets, solutions produced using JPL orbits have the steepest slope in all coordinate components of 8-year solution sets, indicating the most suitable for GNSS-based velocity application of them all. The result from the regression model fit also shows that fixing ambiguities increases the steepness in horizontal components of both 5 and 8-year solution sets when compared to the corresponding ambiguity float solution. Both COD and ESA combined GPS+GLO solution increased the steepness of the regression lines in all the components compared to their corresponding single constellation ambiguity float solution sets. It is also observed, that in both 5 year CODE/ESA and 8-year ESA solution sets, GLO-only solutions have the lowest slop indicating the least precise positioning fix and velocity modeling strategy compared with the rest of the solution sets. One thing to note here is that the outlier points outside the 95%tile regions in Figure 6 and Figure 7 were included in the analysis that yields Figure 8a to Figure 8f.

The findings illustrated in Figure 8a to Figure 8f reveal some outliers in the relationship between the spectral index and velocity uncertainty across certain solution sets and stations, particularly noticeable in the East and Up coordinate components, albeit with minimal impact on the North coordinate component. Notably, these outliers are concentrated at lower latitude stations such as MAS1 (lat = 27.7, lon = 344.3), NKLG (lat = 0.3, lon = 9.6), and POVE (lat = −8.7, lon = 296.1). They predominantly emerge from GLO-only and GPS+GLO solutions derived from COD and ESA 5-year solution sets

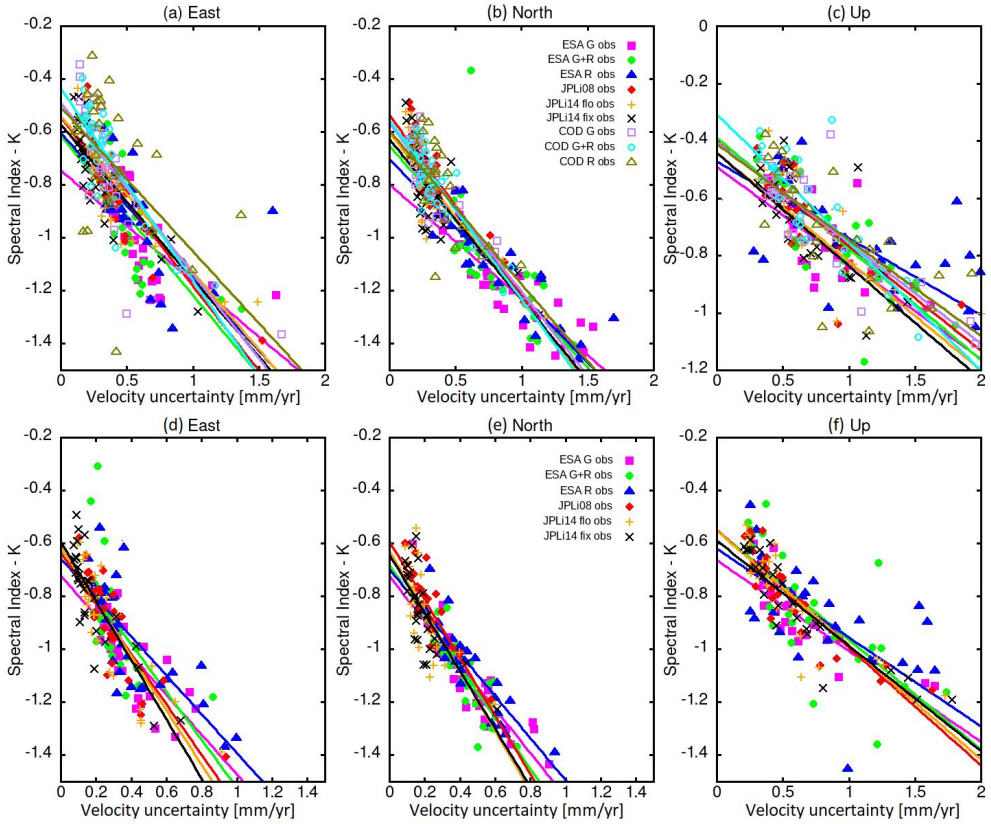


Fig. 8. Linear regression fit between the spectral index and velocity uncertainty from 5 year solution sets in (a–c) and 8 year solution sets in (d–f) estimated using GGM+WN model combination

(Fig. 8a and Fig. 8c) as well as ESA 8-year solution sets (Fig. 8d and Fig. 8f). This disparity suggests a weaker correlation between the spectral index and velocity uncertainty in observations containing GLO at lower latitude stations compared to those at higher latitudes or in GPS-only solution sets across all stations. Alternatively, it could be posited that the noise model combinations utilized in this study inadequately fit the coordinate time series data from such outlier stations. Addressing this would necessitate fitting the coordinate time series to multiple noise model combinations and utilizing the most appropriate noise model for each station's coordinate component data to assess the relationship between spectral index and velocity uncertainty. However, this falls beyond the scope of this study.

The next critical question is, how accurate is the choice of appropriate noise model combination in the velocity and noise level analysis? Is the decision to use the GGM+WN noise model combination to estimate the noise level and velocity uncertainties correct? This could only be answered by assessing the percentage best fit of how well different noise model combinations fit each coordinate component solution data used in this study which is explored in the next section.

### *3.2. Assessment of the appropriate noise model for individual stations' solutions*

To validate that the noise model (GGM+WN) used in Section 3.1 in estimating the noise levels and velocity uncertainties is the best fit for the analyzed solution sets, this study fits all the solution sets to some widely cited noise model combinations. These noise model combinations include the White Noise (WN), combined Power Law and White Noises (PL+WN), combined First Oder Auto-Regressive and White Noises (AR(1)+WN), and a combined Generalized Gauss Markov and White Noise (GGM+WN). The Akaike Information Criterion (AIC) and Bayesian Information Criterion (BIC) values (Akaike, 1974; Schwarz, 1978) are the most widely used criteria in assessing the likelihood of noise model fit on coordinate time series data and they were used in this study. The AIC and BIC values are expressed using Eq. 4 and Eq. 5, respectively.

$$\mathrm{AIC} = 2k + 2\ln(L) \tag{4}$$

$$\mathrm{BIC} = k\ln(N) + 2\ln(L) \tag{5}$$

where $N$ is the number of observations in the time series and $k$ is the sum of parameters in the design matrix, the noise model, and the variance of the deriving white noise process. The $L$ is the likelihood which can be expressed using Eq. 6, according to Bos et al. (2013).

$$\ln(L) = \frac{1}{2}\left[N\ln(2\pi) + \ln\det(C) + 2N\ln(\sigma) + N\right] \tag{6}$$

where $C$ is the covariance matrix and $\sigma$ is the standard deviation of the deriving white noise process.

The highest AIC/BIC values indicate poor fitness of the noise model to the coordinate time series data while the lowest AIC/BIC values indicate best/appropriate noise model fit to the data set. As expected, the WN which is the poorest noise model to fit data generated the highest AIC/BIC values in this study. Relative comparisons were made between the WN and the rest of the analyzed noise model combination by computing the difference between their AIC/BIC values. The computed differences are then converted to percentages. The noise model that returns with the highest percentage of reduction in AIC/BIC values with reference to the WN model is the best fit for that solution set (He et al., 2019).

The number of counts, across all stations used in this study, in which each noise model combination best fits a particular coordinate component solution are stacked together and converted to a percentage and presented as the percentage best fit of that noise model in the solution. The percentage best fitness of how well the analyzed noise model combination each fits the coordinate time series data set used in this study is summarized in Figure 9 for both 5 and 8 year solution sets and in all coordinate components.

In the 5-year solution sets (Fig. 9a), except for JPL orbits floating solutions in the East component, the result shows how GGM+WN has the highest percentage best fit of how the model fits the solution sets in horizontal component based on both AIC and BIC estimates. The JPL floating solutions in the East component are best approximated by AR(1)+WN,

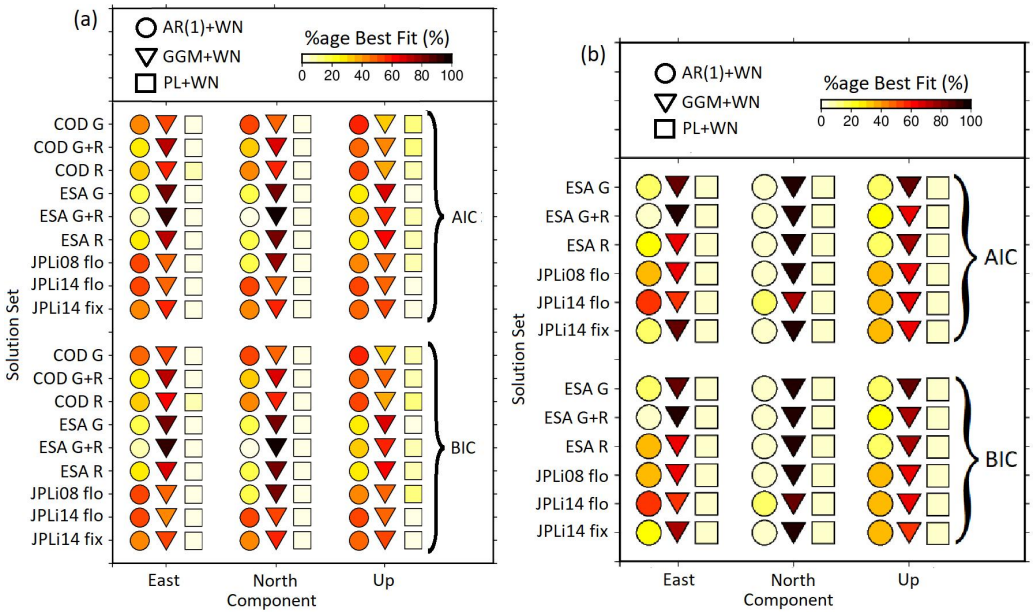


Fig. 9. Percentage best fit of how appropriate the analyzed models fit each 5-year solution in (a) and 8-year solution in (b) time series evaluated using AIC and BIC values. GGM_1mphi coefficient fixed to a value of 6.9e–06

which indicates the best fit of an autoregressive noise model. The Up components of all 5-year ESA and JPL solutions were also best approximated by GGM+WN, except for JPLi14 orbits, which has a 51.6% AR(1)+WN best fit. COD solutions in the Up components were best approximated by AR(1)+WN. In contrast, the COD horizontal components solutions were best approximated by GGM+WN except for the GPS-only solution, which has an AR(1)+WN, which explains the slightly higher noise level estimated than the corresponding GPS+GLO or GLO-only using GGM+WN in Figure 6.

In the 8-year solution sets (Fig. 9b), except for JPL i14 orbits floating solutions in the East component, the result shows GGM+WN noise model combination highly approximated the entire solution sets in all components. The East component's JPLi14 orbits floating solutions have a 50.0% best fit for both GGM+WN and AR(1)+WN noise model combination.

From both Figure 9a and Figure 9b, the results show that increasing the solution time span will reduce the magnitude of autoregressive noise in solution sets, thereby shifting it to a truly GGM+WN model and enhancing the non-stationarity property of the solution sets. Also, resolving ambiguities reduced the best fit of autoregressive noise in solution sets, thereby shifting it to truly GGM+WN as demonstrated by both 5 and 8-year JPLi14 float and JPLi14 fix solution sets. Based on the results shown in Figure 9, the study then justified the choice of the noise model to estimate noise level and trend uncertainties in Section 3.1 is in order.

## 4. Discussion and conclusions

This research investigates the impact of varying coordinate solution time spans, satellite orbit/clock products, and absolute antenna calibrations on the velocity uncertainties and noise magnitude of GNSS stations for appropriate geodynamic studies that require precise velocity estimation. This was achieved by generating a series of PPP solution sets using IGS standard precise orbits and clock solutions from CODE, ESA, and JPL IGS ACs in GipsyX GNSS processing software. The estimated daily station coordinates were organized into time series and were fitted to various noise model combinations to assess the velocity uncertainties and noise magnitude using Hector software. The analyzed results show that:

1. Noise levels are observed to be consistently above –0.7 in 5-year solution sets and below –0.8 in 8-year solution sets. In the Up component, COD and JPL orbits produced solutions with lower noise levels than ESA equivalents, with median values of –0.69 and –0.64. Similarly, JPL orbits provided GPS-only solution sets with a median noise level of –0.77 compared to –0.89 in ESA orbits. JPL on the i08 frame produced less noise in the Up component than JPL on the i14 frame. However, using ambiguity resolution tends to shift the noise from AR(1)+WN to GGM+WN in i14 frame solutions. In all coordinate components, the velocity uncertainties produced by ESA orbits are larger than those produced by COD or JPL orbits. The velocity uncertainties in the Up components are 2 to 3 times higher in magnitude than the average horizontal component. There is an average of 30 and 42% reduction in velocity uncertainties due to 3 years increment in solution span using JPL and ESA orbits, respectively. Combined (GPS+GLO) constellation solution from both COD and ESA reduced the mean values of the velocity uncertainties in all coordinates components compared to their corresponding single constellation (either GPS-only or GLO-only) solution sets.
2. There is a linear relationship between estimated noise levels and velocity uncertainties. The regression analysis between the noise levels and the velocity uncertainties shows solutions produced using JPL orbits have the steepest slope in all coordinate components of 8-year solution sets, indicating the whitest of them all. Solving for ambiguities increases the steepness of horizontal components. Both COD and ESA combined constellation (GPS+GLO) solutions increased the steepness of the regression lines of the solution sets in most of the components compared to their corresponding single constellation solution. Though the GPS-only solutions have the best applicability in geophysical analysis that requires velocity estimation, combined constellation solutions present a good hope provided a longer time span and precise orbit products having less mis-modeling are used.
3. Findings also reveal some outliers in the relationship between the spectral index and velocity uncertainty across GLO-only and GPS+GLO solutions of some lower latitude stations, particularly noticeable in the East and Up coordinate components. This difference implies that there is a less strong relationship between the spectral index and velocity uncertainty in observations including GLO data at lower latitude

stations compared to those at higher latitudes or in solutions solely based on GPS data across all stations.

4. For all the 5-year solution sets in the horizontal component, GGM+WN has the maximum best fit based on AIC and BIC estimates, except JPL orbits floating solutions in the East component. The East component of JPL floating solutions is best approximated by AR(1)+WN, indicating an autoregressive noise model. Except for JPL i14 orbits, which have a 51.6% best fit of AR(1)+WN, all 5-year solutions have a GGM+WN noise model in the Up component. The result also shows that all 8-year solution sets in all components were best approximated by GGM+WN, except JPL i14 orbits floating solutions have a 50.0% best fit for both GGM+WN and AR(1)+WN noise model combinations. Raising the solution time span reduces the magnitude of autoregressive noise in solution sets, resulting in a GGM+WN noise model and increasing non-stationarity properties. Also, resolving ambiguities lowered the best fit of autoregressive noise in solution sets, allowing them to be really GGM+WN.

## Data availability statement

All RINEX observation data used in this study are available in the CDDIS data archive.

## Acknowledgements

I would like to acknowledge the JPL, CODE, and ESA IGS ACs for freely providing the satellite precise orbit and clock solutions used in this study. Thanks to JPL for freely providing GispsyX GNSS processing software license to Modibbo Adama University, Yola which is used in this study. Maps and Figures were generated using Generic Mapping Tools software (Wessel et al., 2019). Thanks to the SEGAL team for freely providing Hector software used in the noise and velocity analysis section of this study.

## References

Akaike, H., (1974). A New Look at the Statistical Model Identification. *IEEE Trans. Autom. Control*, 19(6), 716–723. DOI: 10.1109/TAC.1974.1100705.

Altamimi, Z., Collilieux, X., and Métivier, L., (2011). ITRF2008: an improved solution of the international terrestrial reference frame. *J. Geod.*, 85, 457–473. DOI: 10.1007/s00190-011-0444-4.

Altamimi, Z., Rebischung, P., Métivier, L. et al. (2016). ITRF2014: A new release of the International Terrestrial Reference Frame modeling non-linear station motions: ITRF2014. *J. Geophys. Res. Solid Earth*, 121. DOI: 10.1002/2016JB013098.

Amiri-Simkooei, A.R., Tiberius, C.C.J.M., and Teunissen, P.J.G. (2007). Assessment of noise in GPS coordinate time series: Methodology and results. *J. Geophys. Res. Solid Earth*, 112(B7). DOI: 10.1029/2006JB004913.

Amiri-Simkooei, A.R. (2016). Non-negative least-squares variance component estimation with application to GPS time series. *J. Geod.*, 90(5), 451–466. DOI: 10.1007/s00190-016-0886-9.

Benoist, C., Collilieux, X., Rebischung, P. et al. (2020). Accounting for spatiotemporal correlations of GNSS coordinate time series to estimate station velocities. *J. Geodyn.*, 135, 101693. DOI: 10.1016/j.jog.2020.101693.

Bertiger, W., Desai, S.D., Haines, B. et al. (2010). Single receiver phase ambiguity resolution with GPS data. *J. Geod.*, 84(5), 327–337. DOI: 10.1007/s00190-010-0371-9.

Bertiger, W., Bar-Sever, Y., Dorsey, A. et al. (2020). GipsyX/RTGx, a new tool set for space geodetic operations and research. *Adv. Space Res.*, 66(3), 469–489. DOI: 10.1016/j.asr.2020.04.015.

Bevis, M., and Brown, A. (2014). Trajectory models and reference frames for crustal motion geodesy. *J. Geod.*, 88(3), 283–311. DOI: 10.1007/s00190-013-0685-5.

Blewitt, G., and Lavallée, D. (2002). Effect of annual signals on geodetic velocity. *J. Geophys. Res.: Solid Earth*, 107(B7), ETG 9-1-ETG 9-11. DOI: 10.1029/2001JB000570.

Boehm, J., Niell, A., Tregoning, P. et al. (2006). Global Mapping Function (GMF): A new empirical mapping function based on numerical weather model data. *Geophys. Res. Lett.*, 33(7). DOI: 10.1029/2005GL025546.

Bogusz, J., and Klos, A. (2016). On the significance of periodic signals in noise analysis of GPS station coordinates time series. *GPS Solut.*, 20(4). DOI: 10.1007/s10291-015-0478-9.

Bos, M.S., Fernandes, R.M.S., Williams, S.D.P. et al. (2008). Fast error analysis of continuous GPS observations. *J. Geod.*, 82(3), 157–166. DOI: 10.1007/s00190-007-0165-x.

Bos, M.S., Fernandes, R.M.S., Williams, S.D.P. et al. (2013). Fast error analysis of continuous GNSS observations with missing data. *J. Geod.*, 87, 351–360. DOI: 10.1007/s00190-012-0605-0.

Bos, M.S., Montillet, J.P., Williams, S.D.P. et al. (2020). *Introduction to Geodetic Time Series Analysis*. Geodetic Time Series Analysis in Earth Sciences, pp. 29–52. Springer International Publishing. DOI: 10.1007/978-3-030-21718-1_2.

Calais, E. (1999). Continuous GPS measurements across the Western Alps, 1996–1998. *Geophys. J. Int.*, 138(1), 221–230. DOI: 10.1046/j.1365-246x.1999.00862.x.

Desai, S., Bertiger, W., Fernandez, G.M. et al. (2014). JPL's Reanalysis of Historical GPS Data for the Second IGS Reanalysis Campaign. In American Geophysical Union, Fall Meeting 2014, Abstract #G21A-0427.

Ding, H., Xu, X., Pan, Y. et al. (2020). A Time-Varying 3-D Displacement Model of the ~5.9-Year Westward Motion and its Applications for the Global Navigation Satellite System Positions and Velocities. *J. Geophys. Res. Solid Earth*, 125(4), e2019JB018804. DOI: 10.1029/2019JB018804.

Goudarzi, M.A., Cocard, M., and Santerre, R. (2015). Noise behavior in CGPS position time series: the eastern North America case study. *J. Geod. Sci.*, 5(1). DOI: 10.1515/jogs-2015-0013.

Grapenthin, R. (2020). The Global Navigation Satellite System (GNSS): Positioning, Velocities, and Reflections. https://api.semanticscholar.org/CorpusID:252924970.

He, X., Montillet, J.P., Hua, X. et al. (2017). Noise Analysis For Environmental Loading Effect On Gps Position Time Series. *Acta Geodyn. Geomater.*, 14(1), 131–142. DOI: 10.13168/Agg.2016.0034.

He, M., Shen, W., Pan, Y. et al. (2018). Temporal-spatial surface seasonal mass changes and vertical crustal deformation in south China block from GPS and GRACE measurements. *Sensors*, 18(1). DOI: 10.3390/s18010099.

He, X., Bos, M.S., Montillet, J.P. et al. (2019). Investigation of the noise properties at low frequencies in long GNSS time series. *J. Geod.*, 93, 1271–1282. DOI: 10.1007/s00190-019-01244-y.

Johnson, H.O., and Agnew, D.C. (1995). Monument motion and measurements of crustal velocities. *Geophys. Res. Lett.*, 22(21), 2905–2908. DOI: 10.1029/95GL02661.

Kaczmarek, A., and Kontny, B. (2018). Identification of the Noise Model in the Time Series of GNSS Stations Coordinates Using Wavelet Analysis. *Rem. Sens.*, 10(10). DOI: 10.3390/rs10101611.

Khanzadi, M.R., Mehrpouyan, H., Alpman, E. et al. (2011). On models, bounds, and estimation algorithms for time-varying phase noise. In 5th International Conference on Signal Processing and Communication Systems (ICSPCS), Honolulu, HI, USA, 2011. DOI: 10.1109/ICSPCS.2011.6140897.

Klos, A., Bogusz, J., Figurski, M. et al. (2014). Uncertainties of geodetic velocities from permanent GPS observations: the Sudeten case study. *Acta Geodyn. Geomater.*, 11(3). DOI: 10.13168/AGG.2014.0005.

Klos, A., Olivares, G., Teferle, F.N. et al. (2018). On the combined effect of periodic signals and colored noise on velocity uncertainties. *GPS Solut.*, 22(1). DOI: 10.1007/s10291-017-0674-x.

Kouba, J., and Héroux, P. (2001). Precise Point Positioning Using IGS Orbit and Clock Products. *GPS Solut.*, 5(2), 12–28. DOI: 10.1007/PL00012883.

Langbein, J. (2020). Methods for Rapidly Estimating Velocity Precision from GNSS Time Series in the Presence of Temporal Correlation: A New Method and Comparison of Existing Methods. *J. Geophys. Res. Solid Earth*, 125(7), e2019JB019132. DOI: 10.1029/2019JB019132.

Lyard, F., Lefevre, F., Letellier, T. et al. (2006). Modelling the global ocean tides: modern insights from FES2004. *Ocean Dyn.*, 56(5), 394–415. DOI: 10.1007/s10236-006-0086-x.

Mao, A., Harrison, C.G.A., and Dixon, T.H. (1999). Noise in GPS coordinate time series. *J. Geophys. Res. Solid Earth*, 104(B2), 2797–2816. DOI: 10.1029/1998JB900033.

McCusker, J.R., Currier, T., and Danai, K. (2011). Improved Parameter Estimation by Noise Compensation in the Time-Scale Domain. *Signal Proc.*, 91, 72–84. DOI: 10.1016/j.sigpro.2010.06.008.

Melbourne, W. (1985). The case for ranging in GPS-based geodetic systems. *Proc. 1st Int. Symp. on Precise Positioning with GPS*, 373–386.

Noll, C.E. (2010). The crustal dynamics data information system: A resource to support scientific analysis using space geodesy. *Adv. Space Res.*, 45(12), 1421–1440. DOI: 10.1016/j.asr.2010.01.018.

Petit, G., and Luzum, B.J. (2010). IERS Conventions 2010.

Ries, P., Amiri, N., Heflin, B. et al. (2017). Results from the JPL IGS Analysis Center IGS14 Reprocessing Campaign. Retrieved from https://ui.adsabs.harvard.edu/abs/2017AGUFM.G11B0709R/abstract.

Ries, P. (2019). [IGSMAIL-7837] Completion of JPL IGS14 reprocessing. Retrieved from https://lists.igs.org/pipermail/igsmail/2019/007833.html.

Santamaría-Gómez, A., Bouin, M.N., Collilieux, X. et al. (2011). Correlated errors in GPS position time series: Implications for velocity estimates. *J. Geophys. Res. Solid Earth*, 116(B1). DOI: 10.1029/2010JB007701.

Santamaría-Gómez, A., and Ray, J. (2021). Chameleonic Noise in GPS Position Time Series. *J. Geophys. Res. Solid Earth*, 126(3), e2020JB019541. DOI: 10.1029/2020JB019541.

Schwarz, G. (1978). Estimating the Dimension of a Model. *Ann. Statist.*, 6(2), 461–464. DOI: 10.1214/aos/1176344136.

Singh, G., and Kundu, S. (2022). Outlier and Trend Detection Using Approximate Median and Median Absolute Deviation. In 5th International Conference on Computational Intelligence and Networks (CINE), Bhubaneswar, India, 2022, pp. 01–06. DOI: 10.1109/CINE56307.2022.10037489.

Springer, T., Flohrer, C., Otten, M. et al. (2014). ESA Reprocessing: Advances in GNSS analysis. IGS Workshop 2014.

Sušnik, A., Dach, R., Villiger, A. et al. (2016). CODE reprocessing product series. Astronomical Institute, University of Bern. DOI: 10.7892/boris.80011.

Tregoning, P., and Rizos, C. (2006). Dynamic planet: monitoring and understanding a dynamic planet with geodetic and oceanographic tools. In IAG symposium, Cairns, Australia, 22–26 August 2005.

Wang, L., and Herring, T. (2019). Impact of Estimating Position Offsets on the Uncertainties of GNSS Site Velocity Estimates. *J. Geophys. Res.: Solid Earth*, 124(12), 13452–13467. DOI: 10.1029/2019JB017705.

Wessel, P., Luis, J.F., Uieda, L. et al. (2019). The Generic Mapping Tools Version 6. *Geochem., Geophys., Geosys.*, 20(11), 5556–5564. DOI: 10.1029/2019GC008515.

Wübbena, G. (1985). Software Developments for Geodetic Positioning with GPS Using TI 4100 Code and Carrier Measurements. *Proceedings 1st International Symposium on Precise Positioning with the Global Positioning System*, 403–412.

Zhu, T. (2020). GNSS real-time instantaneous velocimetry based on moving-window polynomial modeling. *IET Radar, Sonar Navig.*, 14(8), 1150–1158(8). DOI: 10.1049/iet-rsn.2020.0035.

Zumberge, J.F., Heflin, M.B., Jefferson, D.C. et al. (1997). Precise point positioning for the efficient and robust analysis of GPS data from large networks. *J. Geophys. Res. Solid Earth*, 102(B3), 5005–5017. DOI: 10.1029/96JB03860.